DISCLAIMER

This report was prepared as an account of work sponsored by an agency of the United States Government. Neither the United States Government nor any agency thereof, nor any of their employees, makes any warranty, express or implied, or assumes any legal liability or responsibility for the accuracy, completeness, or usefulness of any information, apparatus, product, or process disclosed, or represents that its use would not infringe privately owned rights. Reference herein to any specific commercial product, process, or service by trade name, trademark, manufacturer, or otherwise does not necessarily constitute or imply its endorsement, recommendation, or favoring by the United States Government or any agency thereof. The views and opinions of authors expressed herein do not necessarily state or reflect those of the United States Government or any agency thereof. Reference herein to any social initiative (including but not limited to Diversity, Equity, and Inclusion (DEI); Community Benefits Plans (CBP); Justice 40; etc.) is made by the Author independent of any current requirement by the United States Government and does not constitute or imply endorsement, recommendation, or support by the United States Government or any agency thereof.

BNL-227968-2025-TECH
CA/AP/724

Resonant Slow Extraction Simulation using Bmad

B. Dhital

March 2025

Collider Accelerator Department
Brookhaven National Laboratory

U.S. Department of Energy
USDOE Office of Science (SC), Nuclear Physics (NP)

DISCLAIMER

Resonant Slow Extraction Simulation using Bmad

B. Dhital,* K.A. Brown, T. Olsen, and W. Lin
Brookhaven National Laboratory, Upton NY 11973

E. Hamwi, D. Sagan, and G. Hoffstaetter
Cornell University
(Dated: March 28, 2025)

Simulations of slow extraction and transport of charged particle beams from synchrotrons requires careful modeling and experimentation. In this paper, we outline how the Bmad modeling software was adapted and developed to run third-integer resonant extraction simulations of beams at Brookhaven National Laboratory's Booster synchrotron. Further, we show experimental comparisons of the slowly extracted beams transferred to the NASA Space Radiation Laboratory (NSRL) transport line. In this process, beam passes through a stripping foil element at the extraction point, which, along with stripping remaining electrons from the beam ions, acts as a scatterer to modify the phase space, moving to a more Gaussian-like distribution. This modification to the beam helps generate a uniform beam at the beam line's target location; which is necessary for the variety of experiments performed at the facility. During this work, beam energy loss and multiple scattering by foil routines were built in conjunction with the Bmad code developers and are now integrated into the software.

I. INTRODUCTION

The resonant slow extraction method allows for the steady extraction of particles from a synchrotron ring across multiple turns. This extraction process can be analyzed by integrating the various phase-space properties that characterize particle behavior in a synchrotron, especially as the horizontal betatron tune nears a third-integer resonance [1, 2]. At Brookhaven National Laboratory (BNL), this method is applied to extract ion beams from the Booster synchrotron for the NASA Space Radiation Laboratory (NSRL) [3, 4]. The Booster facility provides heavy ion beams of different types over a range of energy levels. The specifics of the Booster ring and the slow extraction approach will be covered in the next section of this paper.

In the following section, we describe a long-term particle tracking program based on Bmad [5, 6], which is used to simulate particles motion through a one-third integer resonance in the Booster synchrotron. The program offers several simulation modes, enabling the study of slow extraction from the Booster ring and subsequent tracking along the NSRL transfer line. We begin with a brief overview of the theory behind one-third integer resonant slow extraction and its implementation in Bmad for simulation purposes. The slow-extracted beam, located at the first septum in the Booster ring, is then transferred to the NSRL beam transport line. These two beamlines are connected via fork and patch elements, which are unique features of Bmad. Additionally, during the development of resonant slow extraction in Bmad, the foil scattering element was implemented for the first time. The slow-extracted beam passing through the foil adopts a transverse Gaussian distribution, and after passing through the constrained optics of the NSRL beamline, it forms a uniform rectangular beam at the NSRL target room, which is used for a variety of experiments by different users.

II. ION TRANSPORT LINE AND ACCELERATOR FACILITIES

A. Ion sources and ion transport lines

A schematic representation of the transport line from the ion source to the NSRL target room is shown in Fig. 1. Three sources supply ions to the Booster and,

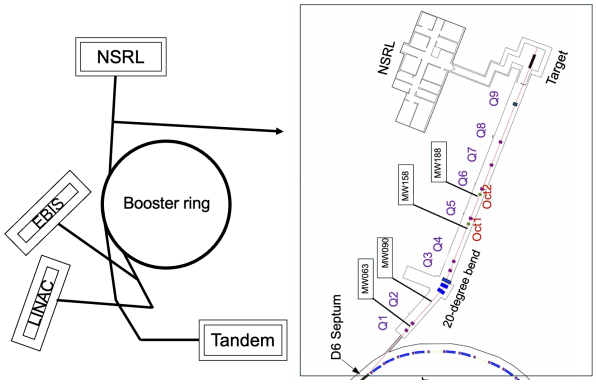

FIG. 1: Layout of the accelerators for NSRL: sources (EBIS, Tandem and LINAC), synchrotron (Booster) and transport segment between the ring and the target room (NSRL-Line) [7].

ultimately, to the NSRL: the LINAC (protons only), the Tandem Van de Graaff (TVDG) which provides protons and selected ions only, and the Electron Beam Ion Source (EBIS) (any ion except protons). The particle beams

* bdhital@bnl.gov

produced by these sources are injected into the Booster synchrotron, where they are further accelerated to the final energy and then delivered to the NSRL via a single transfer line branching from the Booster.

The design of the NSRL facility permit a wide variety of beams to be produced with a great degree of flexibility in the delivery of ion beams to experiments [4]. It includes beams of many ions from protons to thorium, ranging in energy from 50 MeV to 1500 MeV (ion species dependent), and extracted from the Booster accelerator with masses and energies similar to the cosmic rays encountered in space. These ions are delivered to the NSRL from a single beam transport line that branches off from the Booster.

The BNL TVDG operates as a 3-stage type Van de Graaff [8, 9]. An electron is added to a source ion and the negatively charged ion drifts through a large electrostatic potential to a 15 MV HV terminal in the middle of the tank. When passing through the cathode, the previously negatively charged ion becomes positively charged after removing 2 electrons. It continues to accelerate while drifting through the other half of the Van de Graaff tank as it now feels repulsion from the terminal at the middle of the tank. However, the TVDG is unable to supply noble gas sources since attaching the additional electron is not easily achieved. The Brookhaven Linear Accelerator (Linac) operation started in 1971 as a major upgrade to the Alternating Gradient Synchroton (AGS) complex. Its purpose is to provide accelerated protons to the AGS for use in RHIC and to the Brookhaven Linac Isotope Producer (BLIP). The basic components of the Linac include ion sources, a radiofrequency quadropole, and nine accelerator radiofrequency cavities spanning the length of a 459 foot tunnel.

The Linac is capable of producing a negatively charged hydrogen beam of up to 200 MeV of kinetic energy and 135 µA average current. An Electron Beam Ion Source (EBIS) for the Relativistic Heavy Ion Collider (RHIC-EBIS) was commissioned at Brookhaven National Lab in September 2010 and since then it routinely supplies ions for RHIC and the NSRL as the main source of highly charged ions from Helium to Uranium [10].

The workhorse injectors for nuclear physics over the past 40 years, and most recently for the RHIC physics program and NSRL radiobiology and physics programs, were two Tandem van de Graaff accelerators. EBIS has significantly better performance than the Tandems. It consists of an electron beam ionization source, followed by a radiofrequency quadrupole linac and an interdigital-H linac. It resides at the end of 200 MeV proton Linac area and provides all stable ion species from deuterons to uranium, including noble gases such as helium and argon, with much reduced operating costs and greater operational flexibility. EBIS can switch different ion beams to the Booster on a timescale of one second. Table I shows some of ion species with their charge states before and after they are stripped of electrons through foil element, and their mass number respectively. In this paper, we take H ion at 1 GeV kinetic energy to run simulation studies.

TABLE I: NSRL Beam Species

Ion Symbol	Atomic Number	Charge State from Source	Charge State after foil	Maximum Energy (MeV/u)
H	1	-1	+1	2500
He	2	+2	+2	1500
C	6	+5	+6	1000
O	8	+7	+8	1000
Ne	10	+8	+10	1000
Si	14	+11	+14	1000
Ti	22	+17	+22	1000
Fe	26	+20	+26	1000
Kr	36	+18	+36	383
Nb	41	+23	+41	520
Ag	47	+29	+47	575
Xe	54	+27	+54	350
Tb	65	+35	+65	446
Ta	73	+38	+73	386
Au	79	+32	+79	240
Au	79	+43	+79	425
Bi	83	+43	+83	380

Ions for NSRL are extracted from the Booster using slow extraction method. The slow extraction system consists of two septa magnets, five bump magnets, and four sextupole magnets [11–13]. The schematic diagram of five bump magnets, and two septa magnets are shown in Fig 5. The schematic layout of NSRL beam line is shown in Fig. 2. The line consists of three dipoles (D1, D2, and D3) forming a 20° bend, nine quadrupoles (Q1–Q9) magnets, and two octupole (Oct1, and Oct2) magnets respectively. The two octupoles, one upstream of Q5 and the other upstream of Q6, can be adjusted to achieve a uniform rectangular distribution of beam on target. The optics of the line is designed to make an achromatic beam after the two dipoles. This is crucial towards achieving good quality uniform beams since momentum dependent motion at the entrance to the octupoles will affect the uniformity.

B. Booster synchotron

The Booster was designed to accelerate protons and heavy ions [4]. It is a 201.78 m circumference separated function alternating gradient synchrotron that can operate up to a maximum rigidity of 17 T − m. It is composed of 36 sector magnet dipoles and 48 quadrupoles. All magnets are iron-dominated and water cooled. The main dipoles are 2.34 m in (physical) length. Quadrupoles are of two types with (physical) lengths of 0.4255 and 0.4382 m. The vacuum chamber in the dipoles has dimensions 70×150 mm^2 and in the quadrupoles is 152 mm (circular). The nominal betatron tunes are 4.82, horizontal, and 4.83, vertical. The Booster is logically divided into six super-periods, labeled A through F. Each super-

period contains six dipoles and eight quadrupoles, with two long straight sections (the third and sixth locations of every superperiod). These straight sections are used to contain radio frequency (RF) accelerating cavities, injection devices, and extraction devices. For one-third resonance extraction from the Booster ring to the NSRL line, we have five bump magnets, two septa magents and two families of sextupoles placed at different regions of the Booster ring. These sextupole magnets are different than those sextupole magnets being used to correct the chromaticity in the ring. The layout of the Booster ring is shown in Fig. 5.

C. The NSRL facility

The NASA Space Radiation Laboratory (NSRL) at Brookhaven National Laboratory (BNL) was commissioned in October 2002 and became operational in July 2003. The NSRL was constructed in collaboration with NASA for the purpose of performing space radiation research as part of the NASA space program. More detailed descriptions of the design and commissioning of the NSRL facility can be found in Refs. [12, 14]. The

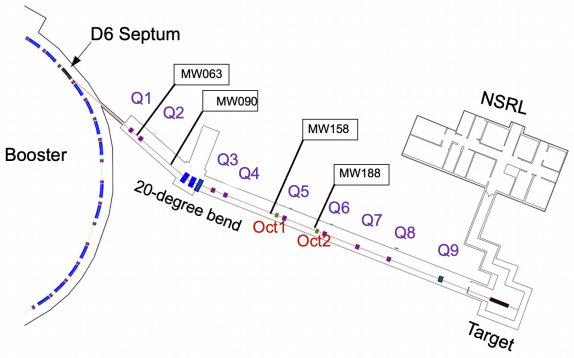

FIG. 2: Layout of the NSRL beam line starting at D6 septum magnet and going downstream to the NSRL target [4].

schematic layout of the NSRL beam line is shown in Fig. 2. The line consists of three dipole magnets forming a 20° bend, nine quadrupoles (Q1–Q9) magnets, and two octupole (Oct1, and Oct2) magnets respectively. The two octupoles, one upstream of Q5 and the other upstream of Q6, can be adjusted to achieve a uniform rectangular distribution of beam on target. The optics of the line is designed to make an achromatic beam after the two dipoles. This is crucial towards achieving good quality uniform beams since momentum dependent motion at the entrance to the octupoles will affect the uniformity.

III. ONE-THIRD RESONANCE EXTRACTION

The slow one-third resonant extraction is a well-established technique used in many accelerator facilities [12, 15] and medical synchrotrons [2, 16–18]. Understanding the dynamics of particle beams during extraction is essential for optimizing accelerator performance. This extraction method involves complex interactions between the beam and the accelerator's magnetic fields. Simulations enable researchers to examine these dynamics in detail, facilitating improvements in extraction efficiency and beam quality.

Resonant extraction can be explained using the stable triangle and the separatrix, which define the stable particles within the synchrotron ring and the unstable particles leaving it. Before initiating the extraction process, the circulating beam must be positioned relative to the resonance. The horizontal tune is gradually shifted closer to the resonance by adjusting the quadrupole magnet currents, while the resonance sextupole is slowly increased to the nominal strength, S, in a quasi-adiabatic manner. Under specific conditions, this results in the deformation of circular trajectories, splitting the phase space into stable and unstable regions, separated by the stable triangle's defining separatrices

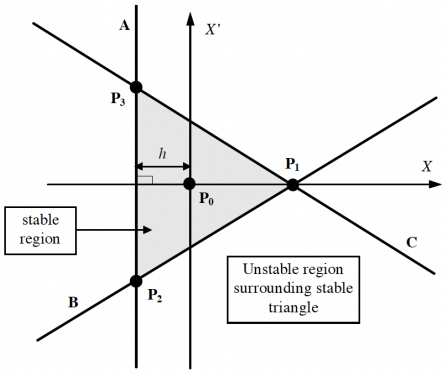

FIG. 3: Geometry of separatrices and stable triangle for a third-integer resonance. Points P_1, P_2, P_3 are three coordinates of a triangle and the three lines A, B, C are three sides of a triangle as described in the ref. [19].

For the slow one-third resonant extraction in the Booster, there are two families of sextupoles, distinct from the chromatic correction sextupoles. Four horizontal sextupoles in the Booster, used for slow extraction, can be powered independently. The extraction resonance is induced by powering these two families of sextupoles with opposite polarities. For a given nominal sextupole field strength S, the size of the stable triangle for a specified tune distance Q is fixed. The stability of a particle with tune Q depends on its initial amplitude in the unperturbed machine.

Now, looking in the Fig. 4, the width of the third-

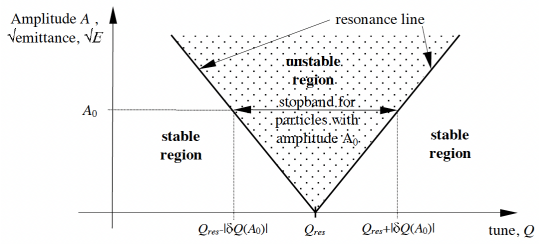

FIG. 4: Steinbach diagram for third order resonance stopband, amplitude-tune space.

integer stopband is symmetric with respect to the resonance. The Steinbach diagram is a plot in amplitude-tune-space where y-axis represents the amplitudes of the particles and the x-axis represents the is tune of the lattice. There are two resonance lines creating a stopband for the particles. All particles falling by any means in between these two resonance lines (dotted unstable region) become unstable and eventually get extracted from the Booster ring. In order to extract particles from the stable region in Fig. 4, they either have to be moved into the unstable region or the size of the unstable region has to be increased. To make particles fall inside the unstable region, we can adjust the following:

- Widening the stopband by increasing the resonance sextupole strength S.
- Moving the particles into the stopband by changing their tune values.
- Increasing the particle amplitudes until the critical value $A(Q)$ is reached.

IV. EXTRACTION SIMULATION

In Bmad, an extraction simulation involves tracking particles through a certain number of turns in a ring and then through an extraction line. In the "INDIVIDUAL" simulation mode, it is assumed that there is a septum, and particles outside the aperture defined by the septum are tracked through the extraction line. Extraction tracking begins with particles that have been labeled 'dead' after crossing beyond the septum, changing their state from'dead' to 'alive', while the remaining particles have their state switched from 'alive' to 'dead'. In this scenario, the D3 septum is modeled as a horizontal kicker magnet, imparting a 3 mrad kick to particles traversing the thin septum wire at the D3 location. Particles that switch their state from 'dead' to 'alive' are then tracked from the D3 septum through to the D6 septum and eventually to the NSRL transport line, reaching the NSRL target location. Before delving into the extraction simulation and particle tracking, we will discuss the special features in Bmad: Branch, Fork, and Patch.

A. Extraction set-up

In this section, the slow extraction set up based on one-third resonant extraction is discussed. We keep the strength S of two families of sextupole in it's nominal value and move the lattice tune through a given tune interval. In this case, one-third resonance tune value is 4.333 (13/3) where we set up lattice tune above 4.333 such that tune distance, $\delta Q = Q_{particle} - Q_{resonance} > 0$. Hence this is the second method as explained above where particles fall into the resonance by changing their tune values. Details on the simulation set up for tune ramping will be explained in section IV C. In our simulation study, we track 1 GeV proton beam of 1000 particles through the Booster ring.

1. *Booster bumps and septa magnets*

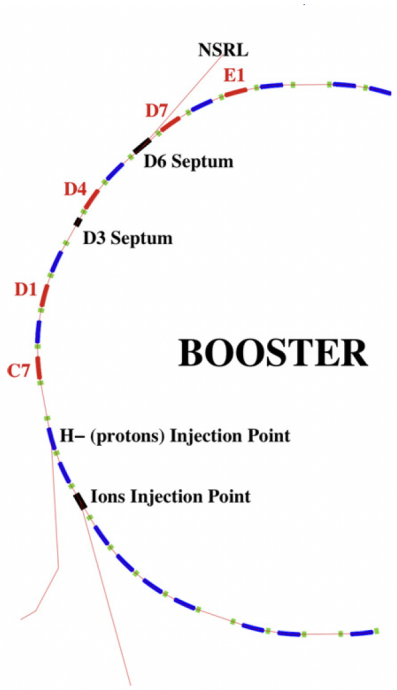

FIG. 5: Locations of NSRL extraction orbit bump magnets and extraction septa magnets.

There are two dipoles septum magnets, D3 and D6 respectively located in the Booster straight sections. The D3 magnet has a very thin (about 0.76 mm thick) wire which is the first crossed by the resonant beam. Having crossed this septum, the ions are deflected by its magnetic field into the magnetic aperture of the D6 thick septum magnet (about 15.2 mm thick), which deflects the particles into the NSRL beamline finally. Just upstream of the D6 magnet, ions that have crossed the D3 septum pass through a foil where the remaining electrons are stripped away. This reduces the ion rigidity thereby

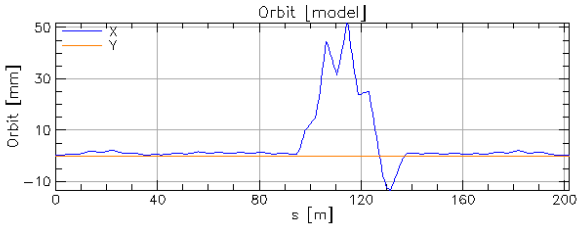

FIG. 6: Equilibrium orbit distortion (in meters) using five bump magnets for extraction from the Booster.

reducing the magnetic field required in the D6 magnet and in the NSRL transport line [4].

As shown in Fig. 6, there are five backleg-winding bumps $C7, D1, D4, D7$ and $E1$ strategically placed along the Booster beam line to distort the equilibrium orbit. Backleg windings create localized perturbations in the primary field of magnet. These perturbations can have different multipoles from the primary field, however in this case they are just dipole perturbations, and cause particles within the beam to experience a slight deviation from their usual trajectory, assisting resonant extraction by shifting the closed orbit closer to the septum.

2. *Extraction sextupole magnets*

In the Booster ring, there are two families of resonant extraction sextupole magnets, with one set being operated in the opposite polarity of the other set. The net effect on the chromaticity of the lattice is, to first order, zero. With this condition established, when particle betatron frequencies reach near 13/3 oscillations/revolution, particle amplitudes begin increasing non-linearly. Over a period of a few hundred to a few thousand revolutions, transverse deviations of particle orbits from the nominal orbit grow sufficiently such that the amplitude from one turn to the three turns later becomes significantly larger than the thickness of the thin septum. Most of the particles step across the septum and enter the magnetic deflection field of the thin septum. Those particles that happen to hit the septum are lost.

B. Simulation set-up using long-term tracking

In the Booster lattice, four extraction sextupoles values are kept to a nominal value and quadrupole tune ramping is applied. "Ramping" is the situation where lattice parameters are changing as a function of time over many turns. In our case, Booster lattice horizontal tune is changing over many turns as a function of the time. Hence for the given sextupole, we ramp quadrupoles only.

The long-term tracking program is for long term (over many turns) tracking of a particle or a beam in a ring. The long-term tracking program can track spin as well as simulate such things as element misalignment, wake fields, higher order mode cavity resonances, energy ramping, beta squeezing, etc. The output of the program will be such things as turn-by-turn particle tracks or beam statistics including beam sizes and polarizations. The long-term tracking program is built atop the Bmad software toolkit. Bmad is a subroutine library for charged–particle and X-Ray simulations in accelerators and storage rings. Hence, Bmad can be used to study both single and multi–particle beam dynamics as well as X-rays.

C. Simulation modes

There are basically two simulation "modes" in a long-term tracking program to run particle tracking in the ring and the transfer line. They are: "SINGLE" and "INDIVIDUAL" modes respectively.

In a "SINGLE" mode, a single particle is tracked for a large number of turns in the ring. A particle with a given amplitude is tracked for many turns until lost or until the maximum number of turns set by user is reached. The output file has particles position for every n turns set by the user. The transverse phase space (x, px) shown in Fig. 7 is at D3 septum location in the Booster ring for five particles with different amplitudes tracked using "SINGLE" mode. D3 septum in the ring is described as a "marker" element and we set this marker as a stop element where all particles position for every n turns are recorded.

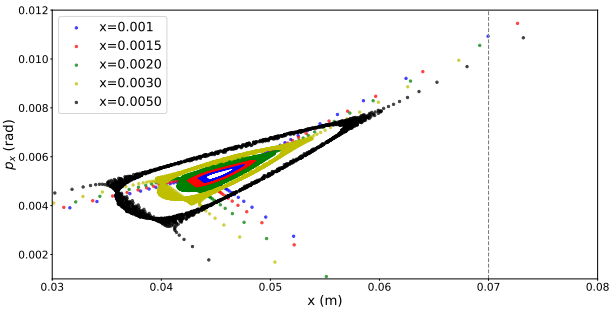

FIG. 7: Transverse phase space of five particles at D3 septum location using "SINGLE" mode.

In an "INDIVIDUAL" mode, a set of particles are tracked one-by-one until lost (or until the maximum number of turns set by the user is reached). The output file has the final coordinates of the particles. The "INDIVIDUAL" mode is useful for the situation when there is ramping and individual are seeing different guide fields due to the time separation between particles. Similar to "SINGLE" mode, "INDIVIDUAL" mode also consider D3 septum as a "marker" element in the lattice and perform a long-term tracking as described above. Instead of treating D3 septum magnet as a "marker" element, we can define D3 septum magnet as a horizontal kicker magnet or as a rectangular bend magnet giving a certain

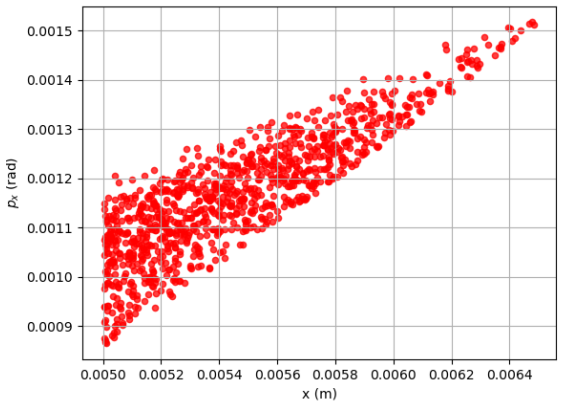

FIG. 8: Transverse phase space particles traversing D3 septum from the beam center using "INDIVIDUAL" mode.

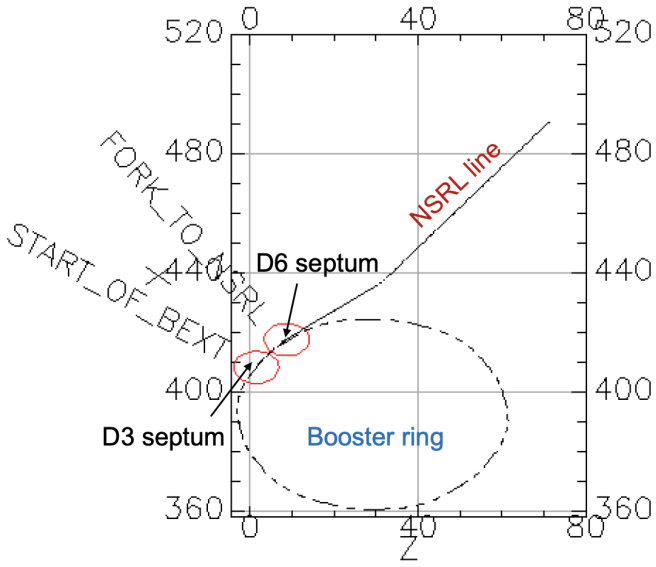

FIG. 9: Connecting Booster ring with transfer lines using fork and patch elements in Bmad.

angular kick to the extracted particles at D3 septum location. This is possible when we consider extraction simulation. An extraction simulation involves tracking particles for some number of turns in a ring and then tracking particles through an extraction line. The details on the extraction simulation will be discussed.

D. Branch, Fork and Patch

A fork element marks the point where multiple lines can merge or branch off from. Forking elements can be used to describe such things as X-ray lines branching from storage rings, injection or extraction lines, etc. In our case, particles hitting at D3 septum location are collected and they get a certain kick at D3 septum. Then another line starting at D3 and ending at D6 septum is forked at D3. The final branch starts at D6 septum location to the end of the NSRL beam line. Hence there are total three branches: one is the Booster ring, second is from D3 to D6 septum, and the third one is from D6 septum to the end of NSRL beam line.

V. SCATTERING THROUGH FOIL

The idea of using the foil along the NSRL beam line has mainly two advantages: first, it reduces the rigidity of the transported beams, and second, the multiple scattering of the ion beams at the foil generates the Gaussian angular distribution which is required for generating a uniform beam distribution at the NSRL target [20]. When charged particles pass through a thin medium foil, the outgoing particles form a Gaussian like angular distribution [21]. In our studies, charged particles are protons and ions at different energies. Scattering process is dominated by screened Coulomb interaction between the projectiles (protons and ions) and target atom (Copper and Aluminium foils). We will discuss the scattering process along with the energy loss mechanism of ions passing through the foil material in the transport line.

A. Scattering angle

We define the scattering angle (σ) following Gerald R. Lynch and Orin Dahl [22]. The expression for the scattering angle becomes

$$\sigma = \frac{S_z z}{p\beta}\sqrt{\frac{X}{X_0}}\left[1 + \varepsilon\, log_{10}\left(\frac{X z^2}{X_0 \beta^2}\right)\right]. \qquad (1)$$

Here p, βc, and z are the momentum, speed, and the charge number of the incident particle, and X/X_0 is the thickness of the scattering medium in radiation length. The other parameters $S_2 = 13.6MeV$ and $\varepsilon = 0.088$ are empirically fitted parameters. For singly-charged ultra-relativistic particles, this form is most accurate at small Z, but at large Z errors can be as large as 11% with respect to a Gaussian fit of the central 98% of the Moliere distribution. Indeed, here we track protons with $\beta \approx 0.87$ through aluminum ($Z = 11$) and copper foils ($Z = 29$) so we are in the region of highest relative accuracy for this approximate form. The Bmad library does also incorporate Lynch and Dahl's own original approximation which we do not further elaborate on here

Further, the beam's angular distribution changes after passing through the foil. If (p_x, p_y) are the transverse momenta of an incoming particle before the foil, then

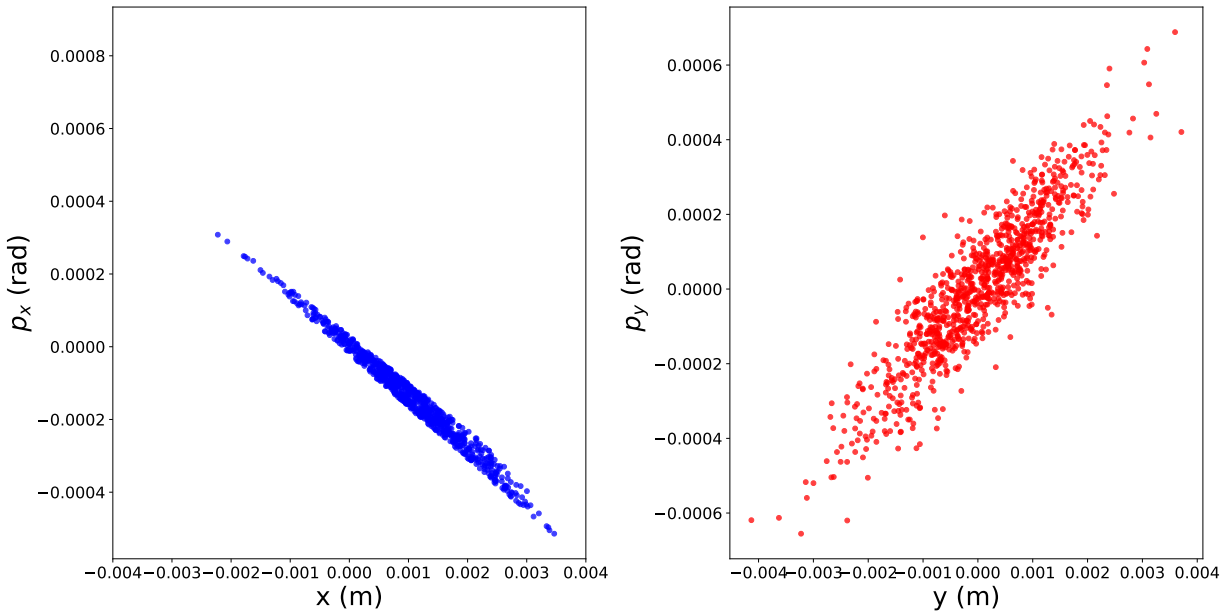

(a)

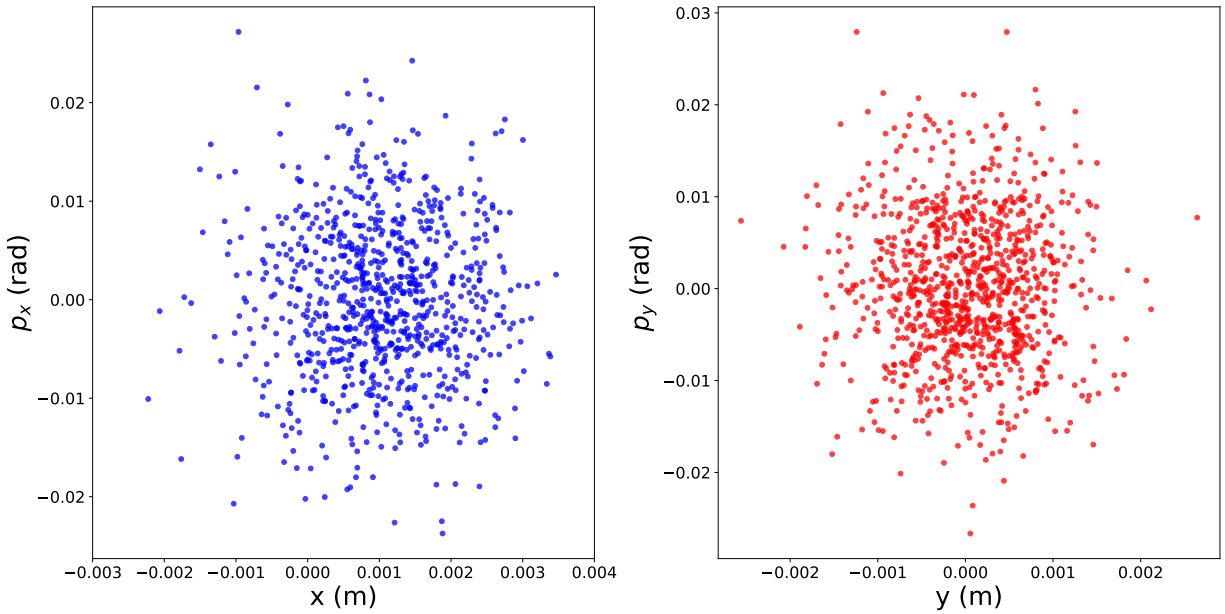

(b)

FIG. 10: Transverse beam distribution (a) Horizontal phase space (x, p_x), and vertical phase space (y, p_y) before D6 septum in the absence of foil. (b) Horizontal phase space (x, p_x) and vertical phase space (y, p_y) after passing through foil at the beginning of the NSRL transfer line.

after foil the new co-ordinates (p'_x, p'_y) become

$$\begin{aligned} p'_x &= p_x + \mathcal{N}(0, \sigma^2)p \\ p'_y &= p_y + \mathcal{N}(0, \sigma^2)p. \end{aligned} \tag{2}$$

Here, $\mathcal{N}(\mu, \sigma^2)$ is a normally distributed random variable with mean μ and variance σ^2. In our simulations we only include the dominating Gaussian component and choose to truncate the $1/\theta^4$ heavy tails of true Rutherford scattering since these particles are likely to be lost in the beam pipe anyway.

Later, the Gaussian beam distribution at the D6 septum (beginning of the NSRL line) as shown in Fig. 10 can be focused magnetically along the beam transport line using a set of different magnets to create a uniform beam at the target.

B. Energy loss through foil

For a particle with speed βc, charge number z, and energy E, traveling a distance x into a foil target of electron number density n and mean excitation energy I, Bmad simulates energy loss according to the relativistic Bethe-Bloch formula [23]

$$\left\langle \frac{dE}{dx} \right\rangle = \frac{4\pi}{m_e c^2} \frac{nz^2}{\beta^2} \left(\frac{e^2}{4\pi\varepsilon_0} \right)^2 \left[\beta^2 - \ln\left(\frac{2m_e c^2 \beta^2}{(1-\beta^2)I} \right) \right], \tag{3}$$

where c is the speed of light, ε_0 is the vacuum permittivity, e, and m_e are electronic charge and rest mass of electron respectively. The electron density n of the material can be calculated by using the following formula

$$n = \frac{N_A Z \rho}{A M_u}, \tag{4}$$

where N_A is the Avogadro number, Z its atomic number, ρ is the density of the material, A is its relative atomic mass, and M_u is the molar mass constant.

Furthermore, Bmad is capable of tracking particles through a wedge-shaped foil, that is, a foil with a linearly varying thickness. The energy loss and scattering angle formulas are adjusted to reflect the local thickness at point of impact for each particle.

Finally, while not relevant for our slow extraction simulation purposes, the Bmad foil element is also capable of stripping ions of any number of their electrons for ring-injection tracking purposes, although the stripping is simulated as a deterministic process with 100% probability.

VI. THE NSRL FACILITY

The NSRL facility at BNL was commissioned in October 2002 and became operational in July 2003. The NSRL was constructed in collaboration with NASA for the purpose of performing space radiation research as part of the NASA space program. More detailed descriptions of the design and commissioning of the NSRL facility can be found in Refs. [12, 14]. The schematic layout of the NSRL beam line is shown in Fig. 2. The line consists of three dipole magnets forming a 20° bend, eight quadrupoles (Q1–Q8) magnets, and two octupole (Oct1, and Oct2) magnets respectively. The two octupoles, one upstream of Q5 and the other upstream of Q6, can be adjusted to achieve a uniform rectangular distribution of beam on target. The optics of the line is designed to make an achromatic beam after the two dipoles. This is crucial towards achieving good quality uniform beams since momentum dependent motion at the entrance to the octupoles will affect the uniformity.

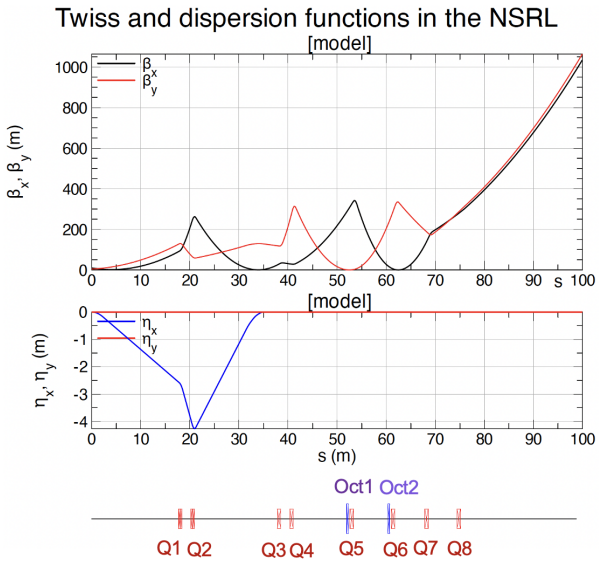

FIG. 11: The horizontal and vertical beta (β_x, β_y), and dispersion (η_x, η_y) functions along the NSRL beam-transport line.

A. Beam line optics and beam constraint

There are basically three constraints in the NSRL beam line optics. The D6 septum magnet, the first two quadrupoles Q1 and Q2, and 20 degree bend dipoles (shown in Fig. 2) form an achromatic bends. The beam is achromatic exiting the end of 20 degree bend dipole magnets. The second constraint is that the (x, x') particle coordinates of the beam at the location of the octupole (Oct1) are highly correlated [24]. A similar constraint at second octupole (Oct2), of highly correlated beam coordinates (y, y'). These constraints are imposed to make sure the beam's uniformity at the target both in horizontal and vertical directions. The NSRL beam line optimization is carried out using Bmad software toolkit to meet these constraints.

B. Creating uniform beams

Inconsistencies in delivering a uniform radiation dose to biological and material samples exposed to charged particle beams present a challenge for researchers [20]. Hence, NSRL target location requires uniform irradiation of materials or biological samples by ion beams. This is achievable following some constraints to the NSRL beamline as discussed in section VI A. The currents in quadrupole magnets are adjusted to get the highly correlated beams in octupoles. These octupoles transform the Gaussian beam into a beam with rectangular cross-section and uniformly distributed particles over the rectangle. The details on the effects of octupoles on the beam

TABLE II: The strength of the magnetic elements corresponding to the first-order beam optics of the NSRL line used to create a uniform beam at the target location with Octupoles ON.

D6 [mrad]	Q1 [m^{-1}]	Q2 [m^{-1}]	D1/D2/D3 [mrad]	Q3 [m^{-1}]	Q4 [m^{-1}]	Q5 [m^{-1}]	Q6 [m^{-1}]	Q7 [m^{-1}]	Q8 [m^{-1}]
155.0	0.255	0.332	0.1164	0.375	0.354	0.246	0.212	0.157	0.005

TABLE III: The theoretical beam parameters at the beginning of the NSRL beam-transport line for 1 GeV proton beams.

α_x	β_x [m]	α_y	β_y[m]	η_x [m]	η'_x	η_y [m]	ε_x^N[mm-mrad]	ε_y^N[mm-mrad]
1.87	10.0	-0.637	4.39	0.0	0.0	0.0	6.33	6.33

distribution is given in Ref. [24]. A more thorough presentation of experimental results from studies of the octupoles in the NSRL is found in Ref. [13]. Figure 12 shows the horizontal and vertical projection of the beam distribution at the target location when octupoles are turned off. The beam distributions are Gaussian which are measured using segmented wire ion chambers (SWICs). Figure 13 shows the beam distributions at the target location when both octupoles are turned on. The projected profiles show that the middle are of the beam distribution is more uniform.

Further, beam size is defined by

$$\sigma_{x,y} = \sqrt{(\varepsilon_{x,y}\beta_{x,y}) + \left(D_{x,y}\frac{\Delta p}{p}\right)^2}, \qquad (5)$$

where $\varepsilon_{x,y}$ is the transverse root-mean-square (RMS) beam emittances, $\beta_{x,y}$ are the horizontal and vertical Twiss beta functions along the beam transport line, $D_{x,y}$ are the dispersion functions and $\Delta p/p$ is the momentum spread of the beam. The NSRL beamline is achromatic after 20 degree bends, and hence there is zero dispersion going downwards to the target. In this case, beam sizes are determined fully by the beam emittances and beta functions along the ring. Based on our measurements with 1 GeV proton beam, the RMS horizontal beam emittance is about 4×10^{-6}mrad [25]. The $\beta\gamma$ value for 1 GeV proton beam is 1.80. The normalized horizontal and vertical emittances are $\varepsilon_N^x, \varepsilon_N^y = 3.5 \times 10^{-6} \times 1.80 =$ 6.33 mm-mrad respectively. Hence the beam profile can be calculated using Eq. 5 and plotted along the NSRL beam line as shown in Fig. 16.

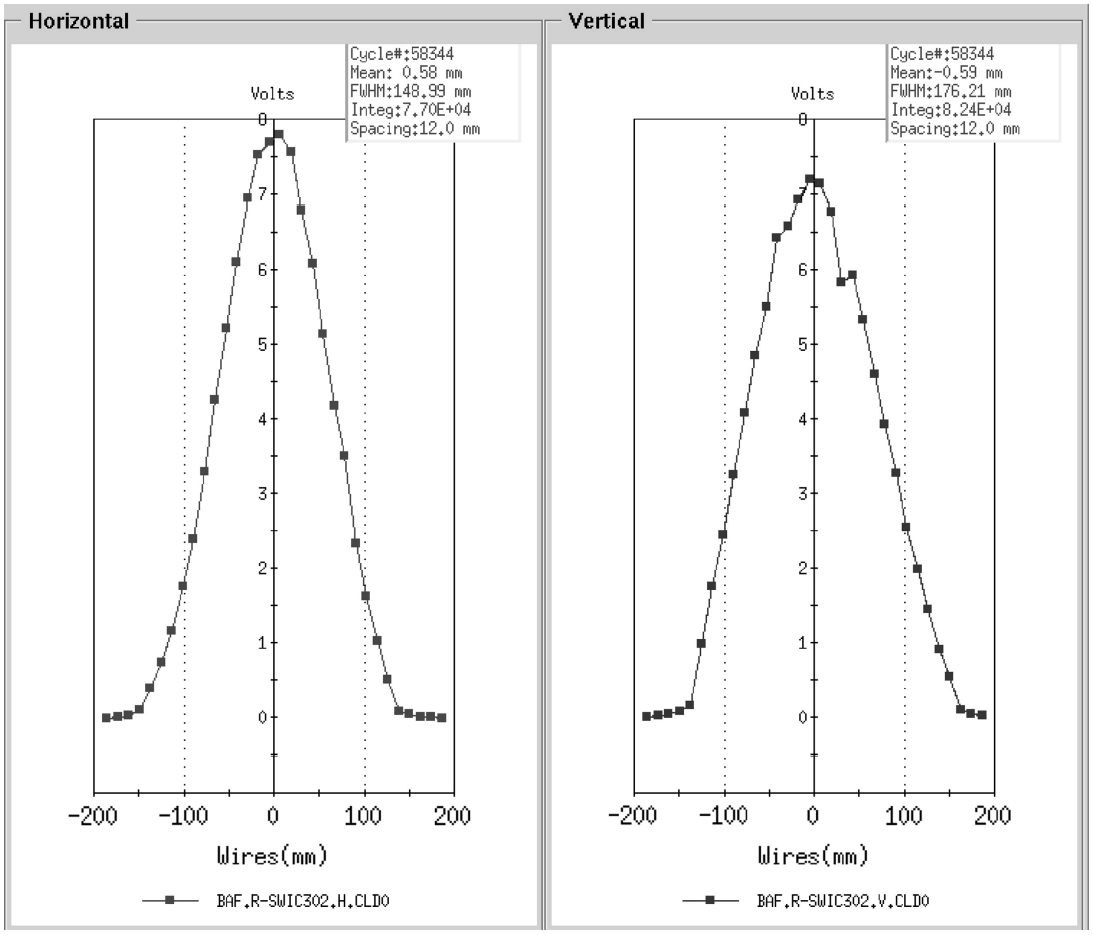

FIG. 12: The horizontal and vertical projections of the beam distribution at the NSRL target location, when the octupoles are OFF.

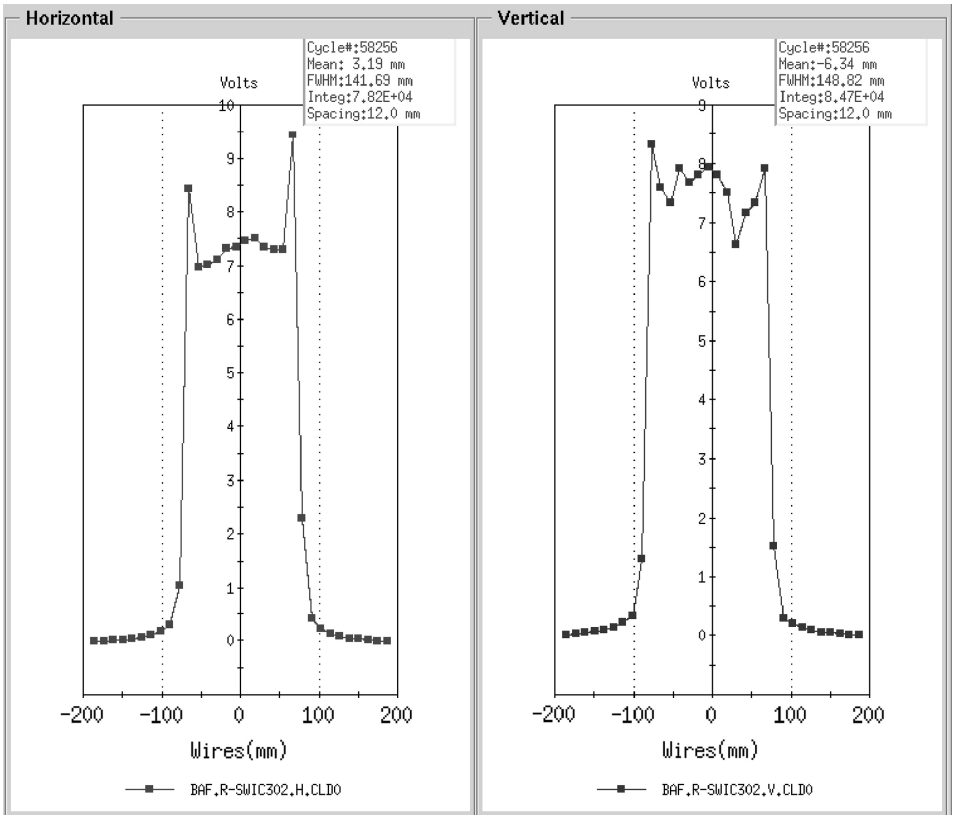

FIG. 13: The horizontal and vertical projections of the beam distribution at the NSRL target location, when the octupoles are ON.

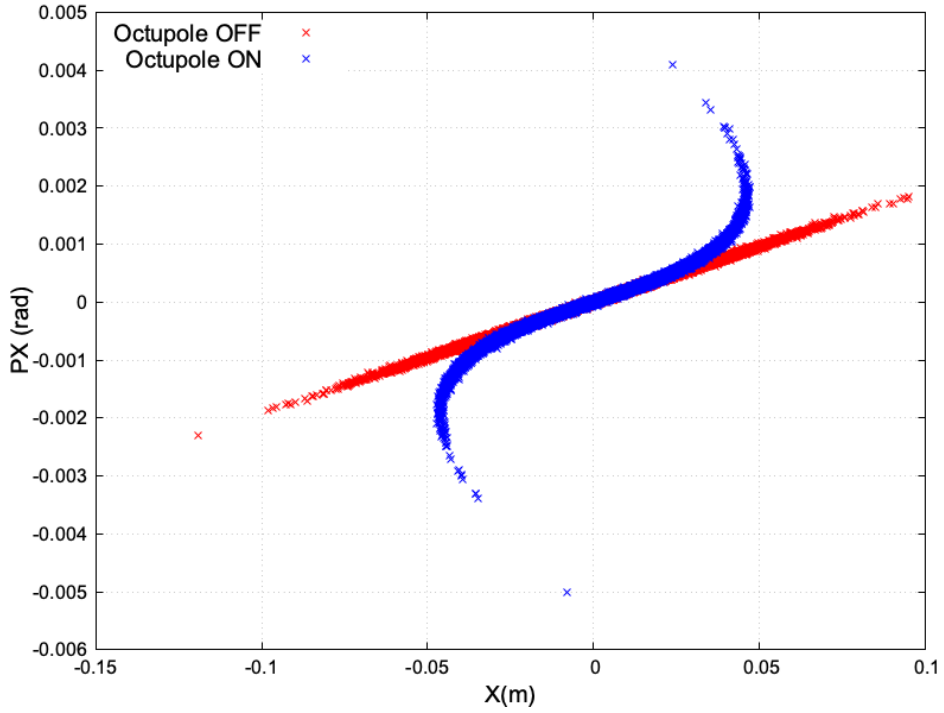

FIG. 14: Horizontal phase-space (x, p_x) distributions of the beam at the target, with horizontal octupole OFF, and ON. This tracking simulation is done in Bmad.

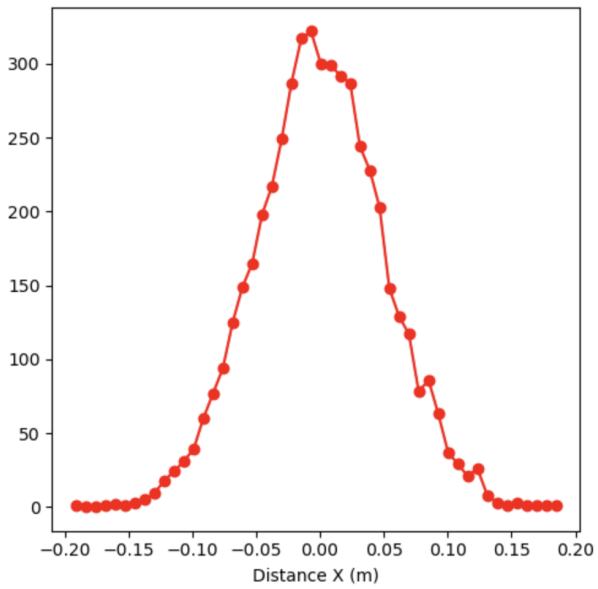

(a) The horizontal projection of the beam distribution at the NSRL target location, when the horizontal octupole is OFF.

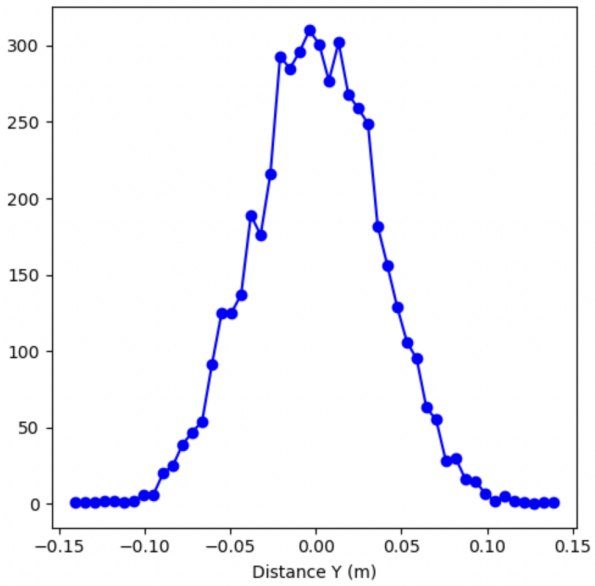

(b) The vertical projection of the beam distribution at the NSRL target location, when the vertical octupole is OFF.

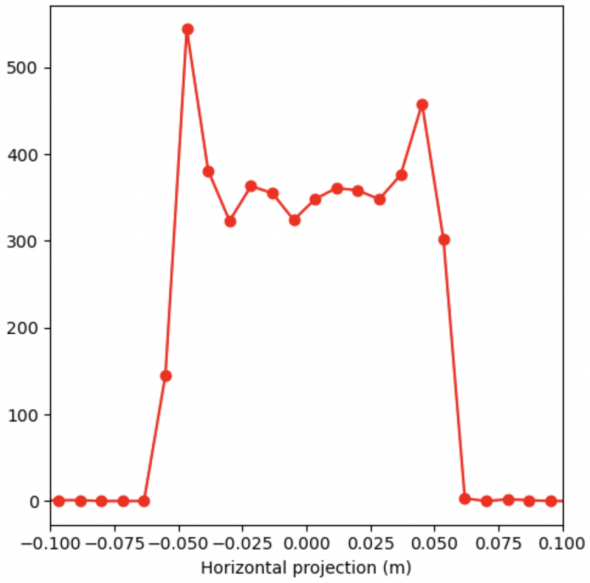

(c) The horizontal projection of the beam distribution at the NSRL target location, when the horizontal octupole is ON.

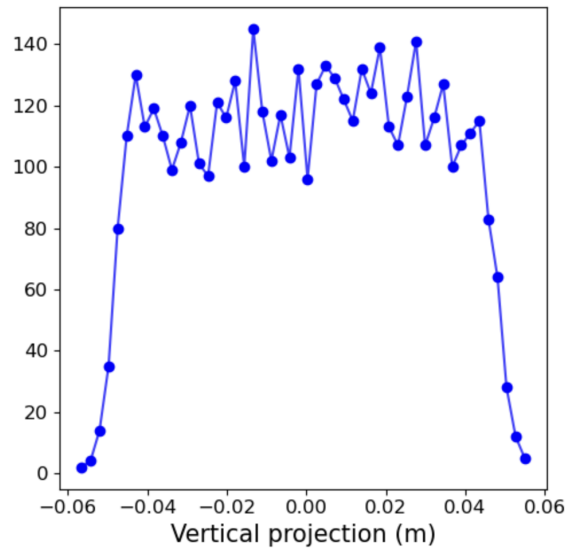

(d) The vertical projection of the beam distribution at the NSRL target location, when the vertical octupole is ON.

FIG. 15: The horizontal and vertical beam distributions at the NSRL target location with Octupoles are OFF and ON respectively (plots are using Bmad).

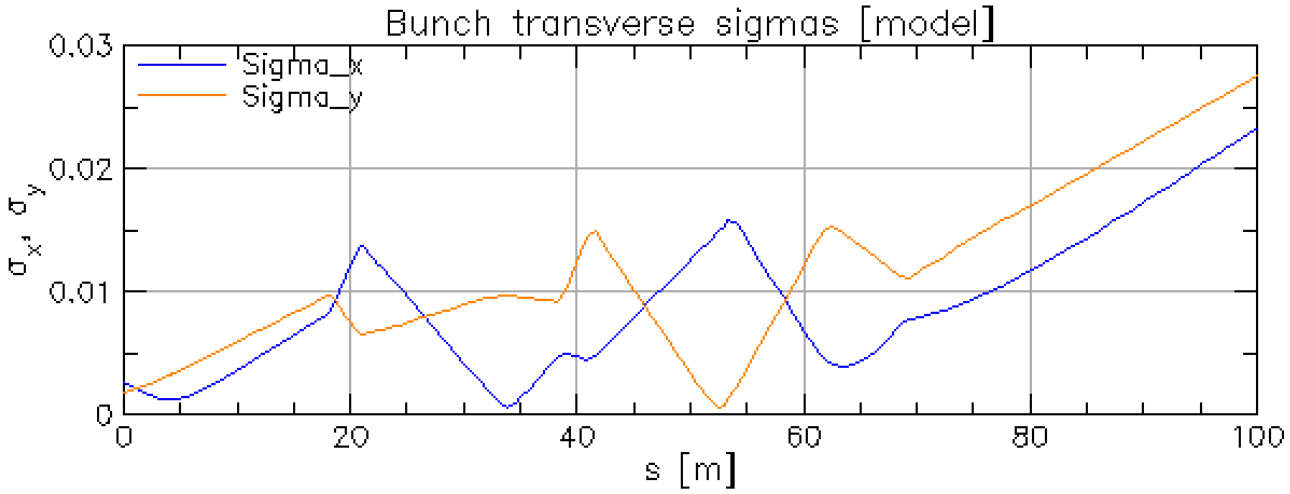

FIG. 16: The horizontal and vertical beam profiles along the NSRL beamline for the given transverse emittance and the Twiss functions.

VII. SUMMARY

The one-third resonant slow extraction in the Booster ring is carried out using Bmad and a particle tracking simulations using a long-term tracking code based on Bmad. Different simulation modes integrated in a long-term tracking program are very useful to completely understand the resonant slow extraction. Further, scattering foil implemented in Bmad for the first time is very useful to understand the beam distribution and energy loss through the foil. The transverse beam distributions passing after scattering foil is Gaussian which is required condition to create a uniform beam at the NSRL target.

VIII. FUTURE WORK

The following are the future work we want to perform in the NSRL beamline

A. Beam line measurement

The magnetic elements and their positions along the NSRL beam line will be measured using a point cloud laser scan that collects data points in a 3D coordinate system, typically captured using LiDAR (Light Detection and Ranging) technology [26]. This method will help for precise alignment verification, dimensional accuracy, and can provide data for simulation and modeling.

B. Digital twin

Based on beamline measurements obtained through Based on beamline measurements obtained through LiDAR scanning, we update the NSRL beamline model to reflect precise alignments and dimensions of the elements. This process ensures that all components match the real-world setup accurately. Following the model update, we build digital twins of the NSRL beamline, creating a virtual representation that mirrors the physical system. This digital twin enables more accurate simulations, diagnostics, and optimization of beam dynamics, contributing to improved beamline performance and efficient future modifications in the NSRL transfer line.

ACKNOWLEDGMENTS

The work is supported by Brookhaven Science Associates, LLC, under Contract No. DE-SC0012704 with the U.S. Department of Energy and by NASA (Contract No. T570X).

[1] M. Q. Barton, Beam extraction from synchrotrons, in *Proc. VIIIth Int. Conference on High Energy Accelerators, CERN, Geneva* (1971) pp. 85–8, https://lss.fnal.gov/conf/C710920/p85.pdf.

[2] M. G. Pullia, Synchrotrons for hadrontherapy, Reviews of accelerator science and technology **2**, 157 (2009), https://www.worldscientific.com/doi/pdf/10.1142/9789814299350_0008.

[3] K. A. Brown, *Third Integer Resonant Extraction: Ripple Compensation and Bunched Beams*, Tech. Rep. (Brookhaven National Lab.(BNL), Upton, NY (United States), 2021) https://www.osti.gov/servlets/purl/1805240/.

[4] K. Brown, L. Ahrens, I. H. Chiang, C. Gardner, D. Gassner, L. Hammons, M. Harvey, N. Kling, J. Morris, P. Pile, *et al.*, The nasa space radiation laboratory at brookhaven national laboratory: Preparation and delivery of ion beams for space radiation research, Nuclear Instruments and Methods in Physics Research Section A: Accelerators, Spectrometers, Detectors and Associated Equipment **618**, 97 (2010), https://doi.org/10.1016/j.nima.2010.02.276.

[5] D. Sagan, Bmad: A relativistic charged particle simulation library, Nuclear Instruments and Methods in Physics Research Section A: Accelerators, Spectrometers, Detectors and Associated Equipment **558**, 356 (2006), https://doi.org/10.1016/j.nima.2005.11.001.

[6] D. Sagan, Long term tracking program (2021), https://www.classe.cornell.edu/bmad/manuals/long_term_tracking.pdf.

[7] C. La Tessa, M. Sivertz, I.-H. Chiang, D. Lowenstein, and A. Rusek, Overview of the nasa space radiation laboratory, Life sciences in space research **11**, 18 (2016), https://doi.org/10.1016/j.lssr.2016.10.002.

[8] P. Thieberger and H. Wegner, The Brookhaven National Laboratory three-stage mp Tandem Van de Graaff facility, Nuclear Instruments and Methods **122**, 205 (1974), https://doi.org/10.1016/0029-554X(74)90483-2.

[9] J. Benjamin, C. Carlson, I. Feigenbaum, M. Manni, D. Steski, and P. Thieberger, Injecting RHIC from the Brookhaven Tandem Van de Graaff, in *Proceedings of the 1999 Particle Accelerator Conference (Cat. No. 99CH36366)*, Vol. 4 (IEEE, 1999) pp. 2277–2279, https://ieeexplore.ieee.org/document/792658.

[10] E. Beebe, J. Alessi, S. Binello, T. Kanesue, D. McCafferty, J. Morris, M. Okamura, A. Pikin, J. Ritter, and R. Schoepfer, Reliable operation of the Brookhaven EBIS for highly charged ion production for RHIC and NSRL, in *AIP Conference Proceedings*, Vol. 1640 (American Institute of Physics, 2015) pp. 5–11, https://www.osti.gov/biblio/1149131.

[11] K. Brown, J. Cullen, J. Glenn, M. Mapes, I. Marneris, N. Tsoupas, L. Snydstrup, and W. van Asselt, Resonant extraction parameters for the AGS Booster, in *PACS2001. Proceedings of the 2001 Particle Accelerator Conference (Cat. No. 01CH37268)*, Vol. 2 (IEEE, 2001) pp. 1517–1519, https://www.osti.gov/servlets/purl/783171.

[12] K. Brown, J. Cullen, J. Glenn, Y. Lee, A. McNerney, J. Niederer, T. Roser, A. Soukas, J. Tuozzolo, and N. Tsoupas, Design of a resonant extraction system for the AGS booster, in *Proceedings of the 1999 Particle Accelerator Conference (Cat. No. 99CH36366)*, Vol. 2 (IEEE, 1999) pp. 1270–1272, https://epaper.kek.jp/p99/PAPERS/TUA83.PDF.

[13] N. Tsoupas, S. Bellavia, R. Bonati, K. Brown, I. Chaing, C. Gardner, S. Jao, I. Marneris, A. Marneris, D. Phillips, *et al.*, Results from the commissioning of the nsrl beam transfer line at bnl, in *Proceedings of the 2004 European Particle Accelerator Conference, Luzern* (2004) https://accelconf.web.cern.ch/e04/PAPERS/THPLT183.PDF.

[14] K. A. Brown, L. Ahrens, I. Chiang, C. Gardner, D. Gassner, L. Hammons, M. Harvey, J. Morris, A. Rusek, P. Sampson, *et al.*, *Performance and Capabilities of the NASA Space Radiation Laboratory at BNL*, Tech. Rep. (Citeseer, 2006) https://accelconf.web.cern.ch/e06/PAPERS/MOPCH099.PDF.

[15] V. Nagaslaev, K. Brown, and M. Tomizawa, Third integer resonance extraction with presence of higher multipoles, Physical Review Accelerators and Beams **22**, 043501 (2019), https://doi.org/10.1103/PhysRevAccelBeams.22.043501.

[16] P. Bryant, L. Weisser, L. Badano, G. Borri, M. Crescenti, P. Holy, S. Reimoser, A. Maier, P. Knaus, M. Pavlovic, *et al.*, *Proton-ion medical machine study (pimms), 2*, Tech. Rep. (CERN/PS 2000-007 (DR), 2000) https://cds.cern.ch/record/449577/files/ps-2000-007.pdf.

[17] F. Kühteubl, E. Renner, L. Adler, L. Fischl, X. German, G. Guidoboni, K. Holzfeind, C. Kurfürst, C. Maderböck, M. Pivi, *et al.*, Investigating alternative extraction methods at medaustron, in *Proceedings of the 14th International Particle Accelerator Conference, IPAC*, Vol. 23 (2023) https://doi.org/10.18429/JACoW-IPAC2023-TUPM091.

[18] M. Regler, M. Benedikt, and K. Poljanc, Medical accelerators for hadrontherapy with protons and carbon ions, Hephy-Pub-757/02 (2002).

[19] M. Pullia, Detailed dynamics of slow extraction and its influence on transfer line design, Diploma of the Doctor's degree, Universite Claude Bernard (1999).

[20] N. Tsoupas, L. Ahrens, S. Bellavia, R. Bonati, K. Brown, I.-H. Chiang, C. Gardner, D. Gassner, S. Jao, W. Mackay, *et al.*, Uniform beam distributions at the target of the nasa space radiation laboratory's beam line, Physical Review Special Topics-Accelerators and Beams **10**, 024701 (2007), http://dx.doi.org/10.1103/PhysRevSTAB.10.024701.

[21] T. Yamazaki, M. Takasaki, and M. Sakisaka, Multiple scattering of protons and nitrogen ions on metal foils, Journal of the Physical Society of Japan **36**, 1643 (1974), https://doi.org/10.1143/JPSJ.36.1643.

[22] G. R. Lynch and O. I. Dahl, Approximations to multiple coulomb scattering, Nuclear Instruments and Methods in Physics Research Section B: Beam Interactions with Materials and Atoms **58**, 6 (1991), https://doi.org/10.1016/0168-583X(91)95671-Y.

[23] F. Salvat, Bethe stopping-power formula and its corrections, Phys. Rev. A **106**, 032809 (2022).

[24] N. Tsoupas, M. Zucker, T. Ward, and C. Snead Jr, Uniform particle beam distributions produced by octupole focusing, Nuclear science and engineering **126**, 71 (1997), https://doi.org/10.13182/NSE97-A24458.

[25] B. Dhital, P. Adams, K. Brown, S. Clark, D. Inzalaco, S. Nemesure, T. Olsen, and N. Tsoupas, An automated quad scan based emittance measurement software, Proc. IPAC'24 , 3447 (2024), https://accelconf.web.cern.ch/ipac2024/pdf/THPG79.pdf.

[26] I. Kim, R. J. Martins, J. Jang, T. Badloe, S. Khadir, H.-Y. Jung, H. Kim, J. Kim, P. Genevet, and J. Rho, Nanophotonics for light detection and ranging technology, Nature nanotechnology **16**, 508 (2021), https://www.nature.com/articles/s41565-021-00895-3.

[27] T. Kanesue, B. Coe, S. Ikeda, S. Kondrashev, C. Liaw, M. Okamura, R. Olsen, T. Rodowicz, R. Schoepfer, L. Smart, *et al.*, *Status of the laser ion source upgrade (LION2) at BNL*, Tech. Rep. (Brookhaven National Lab.(BNL), Upton, NY (United States), 2022) https://www.osti.gov/servlets/purl/1893748.

[28] G. Wheeler, K. Batchelor, R. Chasman, P. Grand, and J. Sheehan, The brookhaven 200-mev proton linear accelerator, Particle Accelerators **9**, 1 (1979), https://www.osti.gov/etdeweb/biblio/5688567.